



Melt polymer drawn single and multi-capillary fibre-based electroosmotic pumps

Liang Wu^{1,2} · Syamak Farajikhah^{3,4,5} · Stephen Beirne¹ · Maryanne C. J. Large³ · Simon Fleming^{3,5} · Peter C. Innis^{1,6} 

Received: 19 July 2021 / Accepted: 27 April 2022 / Published online: 22 May 2022
© The Author(s) 2022

Abstract

Microfluidic devices have been employed in micro-analytical systems and microelectronics using inexpensive, customisable fluid-handling automation at the microliter scale. Here we utilise a well-established fibre drawing technique, which offers a range of materials and capillary conformations, that can be utilized within microfluidic devices to control fluid movement via electroosmotic processes to produce a simple electroosmotic pump (EOP). Single capillary EOPs were fabricated from drawn PU capillary fibres with internal diameters ranging from 73 to 200 μm and were shown to be capable of actively transporting a buffer solution using an external driving electric potential. A maximum flow rate of $0.8 \pm 0.1 \mu\text{L}/\text{min}$ was achieved for a $73 \pm 2 \mu\text{m}$ diameter PU capillary fibre at an applied potential of 750 V/cm. This flow rate was successfully increased up to $5.3 \pm 0.3 \mu\text{L}/\text{min}$ by drawing a multi-capillary array consisting of 4, 5 and 7 capillaries.

Keywords Electroosmotic pumps · Polyurethane (PU) · Microfluidics · Thermally drawn fibres

1 Introduction

Microfluidics (Whitesides 2006) is a technology that enables the manipulation of small volumes of fluid in a precise manner with applications across diverse fields such as DNA analysis (Hosokawa et al. 2004; Wainright et al. 2003), high-throughput screening (Guo et al. 2012), cell biology (Whitesides 2006; Koster et al. 2008), chemical synthesis (Gunther and Jensen 2006), proteomics (Lion et al. 2003) and medical diagnostics (Yager et al. 2006). Underpinning all integrated microfluidic systems is a range of core generic components which include sample delivery capabilities, pumps to move fluid around the device, as well as various other units for combining, mixing, purifying and ultimately detecting of an analyte of interest (Aryasomayajula et al. 2017). An essential function underpinning all of these components is the ability to pump fluid. Micro-pumps with two- or three-dimensional microchannels are frequently utilized in microfluidics as these devices typically have small overall volumes, laminar flow, and a large surface-to-volume ratio. Pumps that utilise electrokinetic flow, such as the electroosmotic pump (EOP), leverage the surface charge which has been described by von Helmholtz (1853) using an electric double layer (EDL) theory (Fig. S1). This surface charge spontaneously develops when a liquid comes in contact with a confined surface within the microchannel or microcapillary and can be used to control fluid movement

✉ Liang Wu
lw654@uowmail.edu.au

✉ Peter C. Innis
innis@uow.edu.au

¹ ARC Centre of Excellence for Electromaterials Science (ACES), Intelligent Polymer Research Institute, University of Wollongong, AHM Facility (Building 231), Innovation Campus, Squires Way, North Wollongong, NSW 2500, Australia

² ARC Centre of Excellence for Electromaterials Science (ACES), School of Nature Sciences I College of Science and Engineering, University of Tasmania, Hobart, TAS 7005, Australia

³ Institute of Photonics and Optical Sciences (IPOS), School of Physics, The University of Sydney, Camperdown, NSW 2006, Australia

⁴ School of Chemical and Biomolecular Engineering, The University of Sydney, Sydney, NSW 2006, Australia

⁵ Sydney Nano Institute, The University of Sydney, Sydney, NSW 2006, Australia

⁶ Australian National Fabrication Facility-Materials Node, University of Wollongong, North Wollongong, NSW 2522, Australia

by controlling the applied electrical field (Xuan 2008; Ghosal 2004, 2006).

Direct current (DC) and alternating current (AC) EOP designs leverage the electroosmotic flow (EOF) process to achieve a laminar pulseless flow profile in a pump configuration which has no moving parts (Wang et al. 2009a, 2009b). The simplicity of the EOP design makes it appealing in applications such as chromatographic separation (Chen et al. 2004) and drug delivery (Chen et al. 2007). The types of EOP designs and their respective applications by other research groups is summarised in Table 1. In these EOP design approaches, microchannels or capillaries are utilised to achieve controllable flow rates (or flow velocity) which are directly controlled via an applied voltage. The majority of these approaches focus on silicon, glass and PDMS for the device fabrication, although there have been reports utilizing thermoplastic polymers (Kirby and Hasselbrink 2004; Nge et al. 2013) such as PU, poly(methyl methacrylate) (PMMA), polycarbonate (PC) and poly(ethylene terephthalate) (PET). The method of fabrication is clearly dominated by lithography (soft lithography and photolithography), involving etching, casting, and bonding, while methods such as hot imprinting and laser ablation have been used to a lesser extent. While there have been extensive developments in the EOP field, both the limitations of material type and fabrication approaches, to some extent, curb the development of EOPs in microfluidic systems.

In this study, for the first time, we develop a cost-effective fibre-based EOP using thermally drawn thermoplastic PU capillary structures fabricated by a well-established fibre drawing technique. This fibre drawing technique has been used previously to produce complex multi-microstructured fibres for photonic devices (Hayashi et al. 2019; Atakaramians et al. 2012; Singh et al. 2012; Tuniz et al. 2013; Eijkelenborg et al. 2001, 2004). The approach is based on rigid polymers and soft glasses, but it can also be used to produce flexible capillary structures with thermoplastic polymers (Fleming et al. 2017; Farajikhah et al. 2021, 2019; Cheng et al. 2015). Here, PU was chosen here as it is flexible, elastomeric and provides an active surface-charged interface. Furthermore, PU has been used in microfluidic devices as a replacement of substance such as silicon, glass and PDMS (Wu et al. 2012; Domansky et al. 2013; Fan et al. 2020). Using the fibre drawing technique, PU capillary fibres with internal diameters ranging from 73 to 200 μm , have been produced and utilised in single capillary and multi-capillary configurations for microfluidic pumping.

2 Materials and methods

2.1 Capillary sample preparation

Continuous PU capillary fibres were drawn from a large thermoplastic PU preform tube (Grayline Inc., USA), having

a 6.4 mm outside diameter, using a fibre draw tower shown in Fig. 1. The drop-off temperature was set to 215 °C while the subsequent drawing was performed at 200 °C. The large PU preform was fed downwards into a furnace at rates between 4 and 25 mm/min, and fibres were drawn with a capstan wheel at rates between 0.5 and 2 m/min. The ratio between the feed and drawing determines the final dimension of the PU capillary fibres. Multi-capillary PU fibres were fabricated using the “stack-and-draw” method, where multiple PU tubes were first arranged into a preform stack, heated to 120 °C for two days and then drawn to fibre as before (Kaysir et al. 2017).

2.2 Characterisation

An optical microscope (Leica M205A) associated with Image J software was employed to measure the cross-sectional and dimensions of the capillary structures. A USB microscope AM4113T-GFBW (Dino-Lite Premier, Clarkson, WA, Australia) equipped with a blue light-emitting diode was used to record the fluid height changes in glass capillary tubes to determine fluid pump rates. A thermal camera (ThermoIMAGER TIM160) was used to record the temperature changes of PU fibres during the tests.

2.3 PU capillary EOPs characterization

A schematic overview of the experimental setup for an EOP is shown in Fig. 2. The EOP design consisted of two reservoirs, the bridging capillary structure and glass capillary tubes for electrode insertion and fluid level determination. The reservoirs consisted of sealable 600 μL microcentrifuge tubes. A Tris-CHES buffer solution, pH 8.83, consisting of 1.0 mM or 5.0 mM Tris-(hydroxyl methyl) amino-methane (Tris) and 1.0 mM or 5 mM N-cyclohexyl-2-aminoethanesulfonic acid (CHES) (Sigma-Aldrich) was used. To accurately determine the flow volumes generated by the EOP, each test was run over 60 s and the head height displacement of the buffer solution was visually observed in the capillary glass tubing recorded over time using a previously reported approach (Hamblin et al. 2007). Flow rates were determined by measuring the change in head height (corresponding to volume) in the glass capillary tubes with respect to time. These capillaries were not involved in controlling electroosmotic flow as no electric field was passed through them. Rather, these capillaries simply measured reservoirs displacement (volume) by changes in capillary head height with respect to time which relates to flow rate. A schematic diagram of the fluid flow in capillary-based EOP was described in our previous work (Wu et al. 2021). Platinum (Pt) wires (30 μm in diameter) were inserted into the top of the capillary tubing in each reservoir to serve as polarizing electrodes. The PU capillary was primed by pressurized

Table 1 The summary of characteristics and applications of EOPs

Material	EOPs design	Microchannel(s) or EOPs Dimensions	Fabrication	Flow rates or flow velocity	Applied voltage (V/cm)	Flow rate/voltage ($\mu\text{L}/\text{min V}$)	Applications (or potential aspects)	Refs.
Glass substrates	A group of (1–100) micro-channels	1–6 μm depth, 4–50 mm length	Photomask, etching	10–400 nL/min	1000	2.00×10^{-3}	A micrototal analysis system (μ -TAS) device	Lazar and Karger (2002)
Silicon (Si) wafer (SiO_2 surface)	An EOP sandwiched by two liquid–gas (lg) separators	Microchannels (10 μm width \times 800 μm length), EOP (100 μm length \times 15 μm width)	Photolithography, Si etching, thermal oxidation, lift-off metallization and anodic bonding	50 $\mu\text{L}/\text{s}$	62.5	6.00×10^{-4}	High density integration into microfabricated fluidic systems	Heuck and Stauter (2011)
PDMS/glass	A liquid metal based EOP	1 cm-length, 30 μm -width, 50 μm -height. chip (3 cm-length, 1.5 cm-width, 3 mm-thickness)	Soft-lithography technique, bonding	10.67 $\mu\text{m}/\text{s}$ (760 $\mu\text{m}/\text{s}$)	25 (1800)	4.56×10^{-5}	Potentially drive cell/macromolecule solutions or drug reagents	Gao and Gui (2014)
PDMS/glass	A multi-stage liquid metal-based EOP	200 μm length \times 40 μm width \times 20 μm height	Soft-lithography technique, bonding	6.26 $\mu\text{m}/\text{s}$ (1.2 mm/s)	1000 (120,000)	2.40×10^{-5}	Potential uses in many high-flow-rate microfluidic applications	Gao and Gui (2016)
Polydimethylsiloxane (PDMS)	Straight micro-channels	100 μm -width, 50 μm -depth micro-channel	Soft lithography technique, bonding	0.07625 $\mu\text{L}/\text{min}$	300	1.27×10^{-4}	For sorting cells	Sun et al. (2007)
Silicon wafer	152 multi-channels EOPs	0.6 mm (Wainright et al. 2003) in volume (40 μm -width, 30 μm -depth)	Lithography, etching, deposition	0.2028 $\mu\text{L}/\text{min}$	20	5.07×10^{-2}	Heat spreader for microprocessor cooling	Eng et al. (2010)
Si substrate	A multi-channel (EOF)	$L_1 = 50 \mu\text{m}$, $d_1 = 5 \mu\text{m}$	MEMS technology (patterning, bonding)	38 $\mu\text{L}/\text{min}$	8000	9.5×10^{-1}	Thermal management of stacked chips (3D-Ics)	Kudo et al. (2014)
PDMS	3D parallel (EOF) pump	10,500 μm -length, 116 μm -width	Soft photolithography, bonding	5.69 nL/min	1.90	2.84×10^{-3}	Potential biological analysis and drug delivery systems	Ye et al. (2019)
Polyurethane (PU)	Microchannels	1 cm-length, 150 μm -width, 500 nm to 80 μm -heights	Photolithography, casting, bonding, peeling	$2.47 \times 10^{-8} \text{ m}^2/\text{Vs}$	200	14.8	Blood contacting applications	Wu et al. (2012)
Polycarbonate (PC)	Microchannels	178 μm -length, 72 μm width (top) and 28 μm width (bottom), 31 μm depth	Hot Imprinting, laser ablation method, thermal sealing	$7.0 \times 10^{-4} \text{ cm}^2/\text{Vs}$	1160	6.03×10^{-3}	Rapid microfluidic mixing	Johnson et al. (2002)

Table 1 (continued)

Material	EOPs design	Microchannel(s) or EOPs Dimensions	Fabrication	Flow rates or flow velocity	Applied voltage (V/cm)	Flow rate/voltage ($\mu\text{L}/\text{min V}$)	Applications (or potential aspects)	Refs.
Poly(ethylene terephthalate glycol) (PETG)	Trapezoidal channels	2 μm -depth, 1.8 cm-length	Laser ablation, hot imprinting	$5.6 \times 10^{-4} \text{ cm}^2/\text{Vs}$	300	60.48	A micrototal analysis systems ($\mu\text{-TAS}$)	Henry et al. (2002)
Cyclic olefin copolymer (COC)/silicon nanostructures	Rectangular microchannel with silicon nanostructures on the bottom	100 μm -width, $4.8 \pm 0.1 \text{ cm}$ -length	Dry etching, electroplating and moulding	$9.06 \times 10^{-4} \text{ m/s}$	100	225.9	Chemical and biological analyses	Lim et al. (2018)
Polyurethane (PU)	Microchannels	28 μm -depth, 60 μm -width, 4.0 cm-length	Photolithography and nickel electrodeposition	$3.2 \times 10^{-4} \text{ cm}^2/\text{Vs}$	500	76.8	The separation of epinephrine and l-3,4-dihydroxyphenylalanine coupled to end-column amperometric detection	Piccin et al. (2007)
PDMS/glass	Microchannels	50 μm -depth, 100 μm -width, 20 mm-length	Photolithography, wet chemical, and soft lithography	60–80 $\mu\text{m/s}$	25	$7.2 \times 10^{-4} \sim 9.6 \times 10^{-4}$	Microfluidic point-of-care blood analysis	Mohammadi et al. (2015)
PDMS/glass	Microchannels	50 μm -depth, 50 μm -width, 5 cm-length	Soft lithography	0.15 $\mu\text{L}/\text{min}$	130	2.30×10^{-4}	Microfluidic device for bacteria isolation	Miller et al. (2019)
Poly(methyl methacrylate) (PMMA) and PC	Microchannels	80 μm -depth, 50 μm -width, 4 cm-length	Lithography, electroforming and micromolding	$5.0 \times 10^{-4} \text{ cm}^2/\text{Vs}$	150	120	Cell transport	Witek et al. (2004)

Fig. 1 Schematic of fibre drawing process (inset: a typical temperature profile inside a fibre drawing furnace with respect to the preform position)

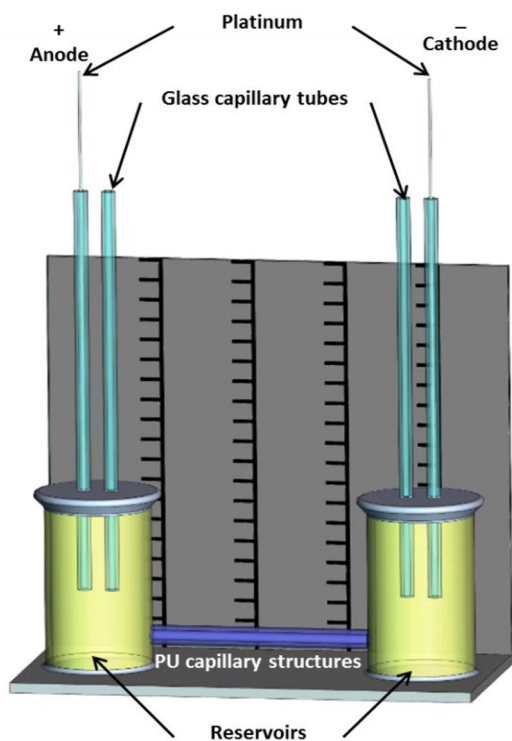
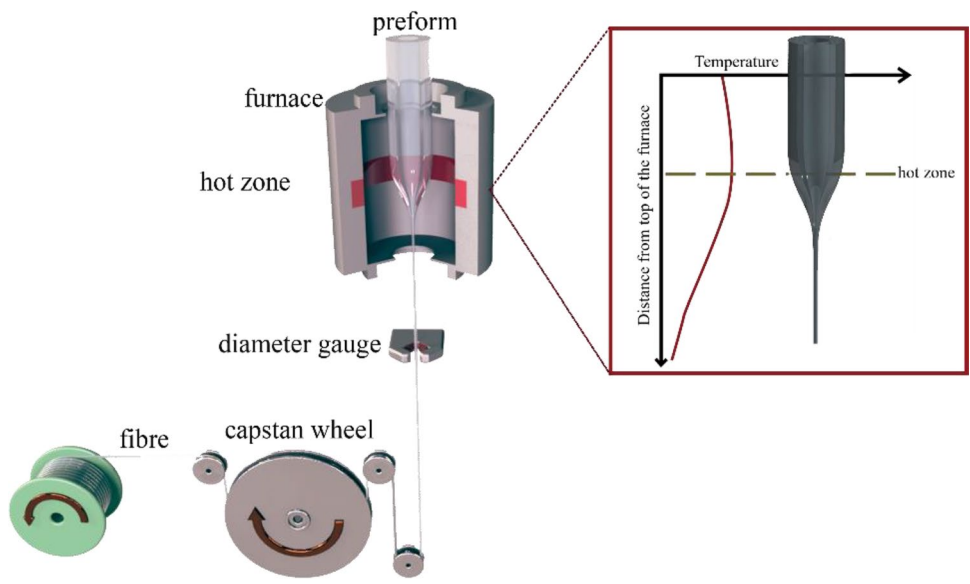
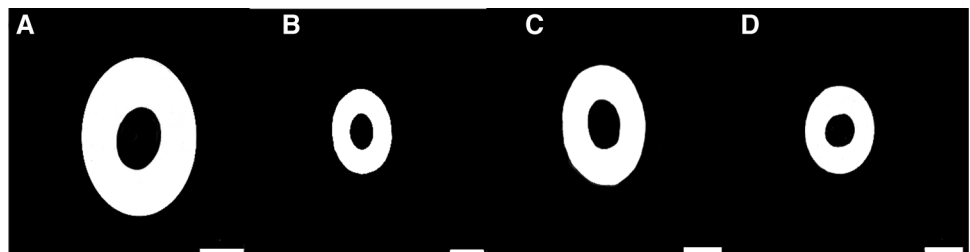


Fig. 2 A schematic overview of capillary EOPs

Fig. 3 Optical micrographs of the PU single-capillary structures with **A** 200 μm , **B** 160 μm , **C** 93 μm and **D** 73 μm internal diameters (the scale bar is 200 μm for **A** and **B**, and 100 μm for **C** and **D**)



injections of the buffer solution into the reservoir to ensure removal of air blockages within the capillary channel. A LabSmith HVS448 High Voltage Sequencer ($3\text{ kV} \pm 0.05\%$) was used to apply an electric field of up to $\pm 1500\text{ V}$. PU capillary of 20 mm in length were tested in triplicate at applied fields up to the 1500 V supply limit.

3 Results and discussion

3.1 Morphology characterisation of PU capillary structures

3.1.1 PU single-capillary fibres

PU capillary fibres with inner diameters ranging from approximately 73–200 μm were successfully fabricated, as shown in Fig. 3. The resultant micro-channels (capillaries) were observed to have mainly ovoid-circular cross-sectional capillary shape. Deviations from circularity result from the original preforms being non-circular due to manufacture and/or storage deformation. The data describing the characteristics of the capillary area and structures for these PU capillary samples are given in Table 2. The inner diameters

of the capillary structures were in the range of 73–200 μm , while the outer diameters of these samples were between 172 and 523 μm . The cross-section area of the PU capillary was from 4 to $33 \times 10^3 \mu\text{m}^2$, compared with the whole structure cross-sectional area 22– $420 \times 10^3 \mu\text{m}^2$. The area ratio of the inner capillaries to the whole fibre structures was between 15.4% and 18.7%.

3.1.2 PU multi-capillary fibres

PU capillary fibres with different numbers of capillaries were also investigated. The cross-sectional images of these samples with 4, 5 and 7* capillaries are shown in Fig. 4. These capillaries were distributed based on the preform stacking configuration resulting in triangular (Fig. 4A), rectangular (Fig. 4B) and hexagonal formats (Fig. 4C). The structural analysis of the resultant cross-sections of the drawn capillary structures is given in Table 3. As a consequence of the drawing process, a clear distortion of the capillaries was

noted resulting in a range of non-circular capillary shapes. For example, the width of these capillaries in Fig. 4A was $54 \pm 16 \mu\text{m}$, while the height was between $36 \pm 12 \mu\text{m}$. The cross-section area of the capillaries was $7379 \mu\text{m}^2$, compared with the cross-sectional area of the whole fibre $39,000 \mu\text{m}^2$. The area ratio of the multi capillaries to the whole fibre structures was between 10.7 and 18.9%.

The number of functional capillaries in the multi-capillary structure in Fig. 4C was actually 13, with 7 large and 6 small capillaries. However, here the six smaller capillary channels were considered to have a negligible effect on the overall flow rate due to their relative size when compared to the larger seven capillaries. Therefore, the number of functional capillaries was considered to be 7* in this configuration.

3.2 Flow properties of PU capillary EOP

PU capillary EOPs of 20 mm in length were tested over a 60 s period using a 1 mM Tris-CHES buffer at ± 200 to ± 1500 V. Electrical current is typically used to monitor the EOF in microfluidic devices (Locascio et al. 1999; Pittman et al. 2003; Huang et al. 1988), as it reflects the real-time EOF within the capillaries under different experimental conditions. Here, the resultant device currents were observed to increase with an increasing voltage, Fig. 5. Similar current trends were also observed for EOPs with different diameters, Fig. S2A–C. Furthermore, the observed currents increase as the diameter (or area) increase when the same voltage was applied as seen in Fig. S2D. In addition, the observed current was related also to the concentrations of buffer where

Table 2 The dimensions of PU single-capillary structures

Material-structure	PU capillary			
	1	2	3	4
Samples	1	2	3	4
Capillary structure overall area ($\times 10^3 \mu\text{m}^2$)	215	107	39	22
Capillary area ($\times 10^3 \mu\text{m}^2$)	33	20	7	4
Capillary/structure area ratio	15.4%	18.7%	18.0%	18.2%
Capillary inner diameter (μm)	200 ± 5	160 ± 2	93 ± 6	73 ± 2
Capillary outer diameter (μm)	523 ± 8	368 ± 10	224 ± 6	172 ± 3

Fig. 4 Optical micrograph of the PU multi-capillary structures **A'** 4-capillary before melting, **B'** 5-capillary before melting, **C'** 7-capillary before melting, **A** 4-capillary after melting, **B** 5-capillary after melting, **C** 7*-capillary after melting (the scale bar is 200 μm)

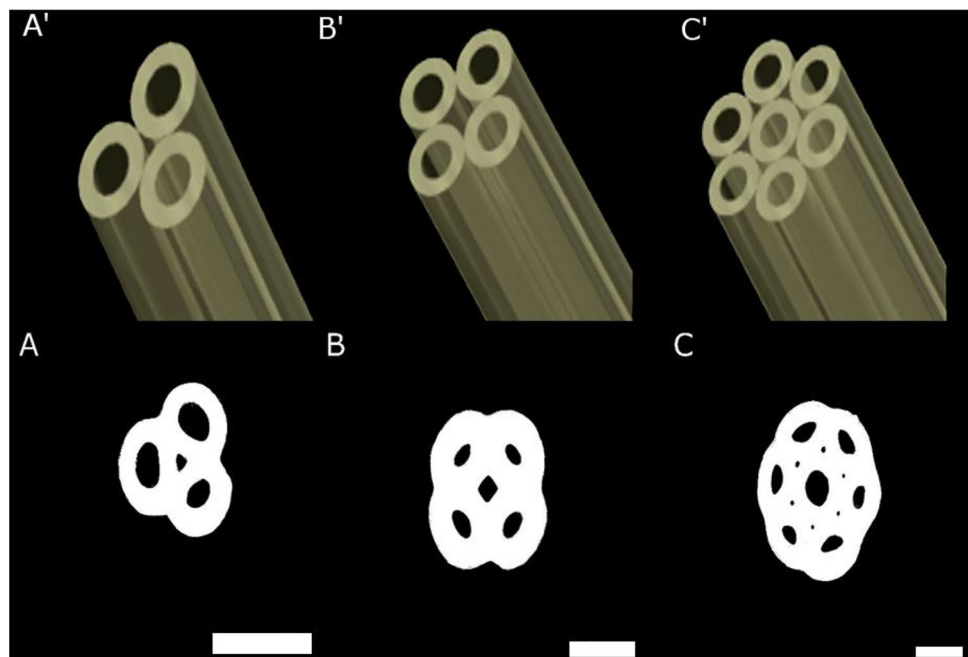


Table 3 The dimensions of drawn PU multi-capillary structures

Material-structure	PU multi-capillary			
	The number of capillaries			
	4	5	13	
			7*	6
Capillary average area ($\times 10^3 \mu\text{m}^2$)	1.8	2.4	4.7	0.3
Capillary structure overall area ($\times 10^3 \mu\text{m}^2$)	39	112	241	
Capillary overall area ($\times 10^3 \mu\text{m}^2$)	7.4	12.0	33.0	1.3
Capillary/structure area ratio	18.9%	10.7%	14.3%	
Capillary width (μm)	54 ± 16	60 ± 10	96 ± 19	13 ± 3
Capillary height (μm)	36 ± 12	40 ± 8	57 ± 17	9 ± 2

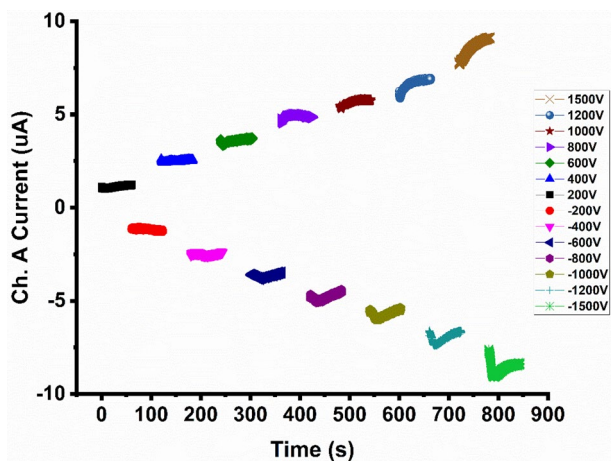


Fig. 5 The flow properties of 200 μm PU-EOPs at different applied voltages versus time

the higher the concentration resulted in a higher current response, Fig. S2D.

The current responses observed for various voltages, geometries, and buffer solutions in the EOP can be described by EDL theory. The electrical current, I , can be expressed by the relationship in Eq. 1;

$$I = \frac{\kappa \times E \times A}{L}, \tag{1}$$

where E is the electrical field strength applied to the capillary, κ is the ionic conductivity in the solution, A is the cross section of the capillary ($A \propto d^2$), where d is the diameter of capillary) and L the length of capillary. A lower current would be expected with decreasing capillary area, increasing capillary length, reducing voltage and conductivity of buffer solution. Importantly, in a practical device, a lower current would be advantageous as it would assist in minimising localised Joule heating which would result in non-linear flow behaviour by inducing viscosity and ionic mobility changes (see discussion below) (Xuan 2008; Ghosal 2006; Grushka et al. 1989). PU-EOP samples with a 73 μm diameter gave a relatively stable performance with

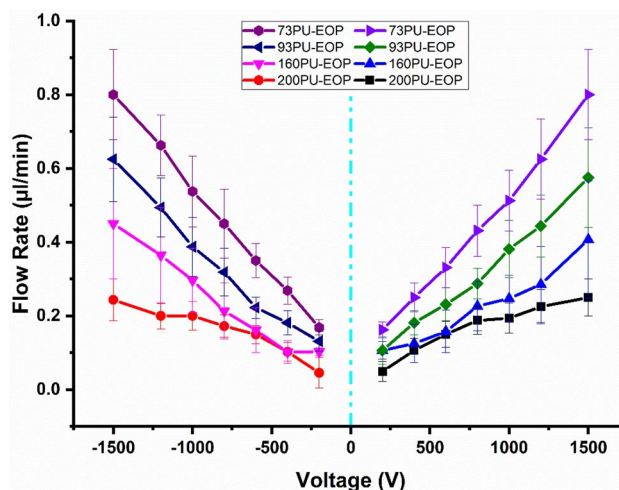


Fig. 6 The flow rates of PU-EOPs with different diameters versus voltages

respect to current variations observed during operational tests, Fig. S2A.

3.2.1 EOP flow rate

The flow rate (or electroosmotic velocity) of the electrolyte within the PU capillary EOP was determined by measuring the changes in the liquid head height in microcapillary glass tubes with respect to time. The dependence of the flow rate with respect to the applied voltage, Fig. 6, ideally should increase linearly with electric field as predicted by Eq. 5 (see ESI Sect. 1.1), where velocity (u) was influenced by the electric field (E). However, EOPs with a larger capillary cross section, such as the 200 μm -EOP, were significantly affected by the operational temperature (as a result of Joule heating) as well as the presence of electrolysis bubbles that were generated at higher voltages which could travel more readily inside the larger capillary sizes. As a result, the larger capillaries exhibited a more unstable and non-linear performance when compared to the 73 μm EOP (with respect to the

observed current at the same applied voltage, Fig. 5 and Fig. S2). There was also a clear trend of the flow rate decreasing with respect to the increase in capillary diameter, Fig. 6. This behaviour is not predicted by Eq. 5 (see ESI Sect. 1.1) where the flow rate is proportional to the cross-sectional area of the capillaries. One reason for this may be due to an influencing competitive and counteractive siphon effect. This is in line with the report of Wim Kok that siphoning is not a problem with diameters of $\leq 50 \mu\text{m}$, but is stronger in wider capillaries $\geq 100 \mu\text{m}$ (Kok 2000). This effect can dramatically offset the driven force generated by the electric field when the diameter of capillary increased. Significantly, the PU EOP of $73 \mu\text{m}$ in diameter exhibited a significant pumping performance ($0.8 \mu\text{L}/\text{min}$ at 1500 V or $5.33 \times 10^{-4} \mu\text{L}/\text{min V}$) when compared to a reported silica-based EOP (Dasgupta and Liu 1994) with a flow rate of $3.33 \times 10^{-5} \mu\text{L}/\text{min V}$ and PDMS-based EOPs (Gao and Gui 2014) with a flow rate of $4.56 \times 10^{-5} \mu\text{L}/\text{min V}$, as shown in Table 1.

3.2.2 Thermal properties of PU capillary EOP

Joule heating resulting from the passage of electric current through a capillary filled with a resistive electrolyte media, is problematic, particularly when higher voltages are applied. The impact of Joule heating on the PU capillary was investigated over $400\text{--}1500 \text{ V}$, Fig. 7. In Fig. 7C, D, the temperature of PU-EOPs upon the application of a driving voltage at 20 s increased dramatically—reaching a relatively steady rate until the end of the experiment (at 80 s). The heat generated was observed to decrease rapidly to the ambient temperature once the driving voltage was removed. The maximum temperature change ($\Delta T = 3^\circ\text{C}$) was observed using a thermal imaging camera for the $200 \mu\text{m}$ -EOP at 1500 V , while the $160 \mu\text{m}$ -EOP was slightly lower at 1.2°C . Significantly, there was no observable temperature change (ΔT) for the $73 \mu\text{m}$ and $93 \mu\text{m}$ EOP. The observed temperature differences were directly related to the observed current during the EOP operation. Here, the current was related to the inner diameter, d , (or area) of the capillary, where $I \propto d^2$. Therefore, a smaller volume capillary will result in lower

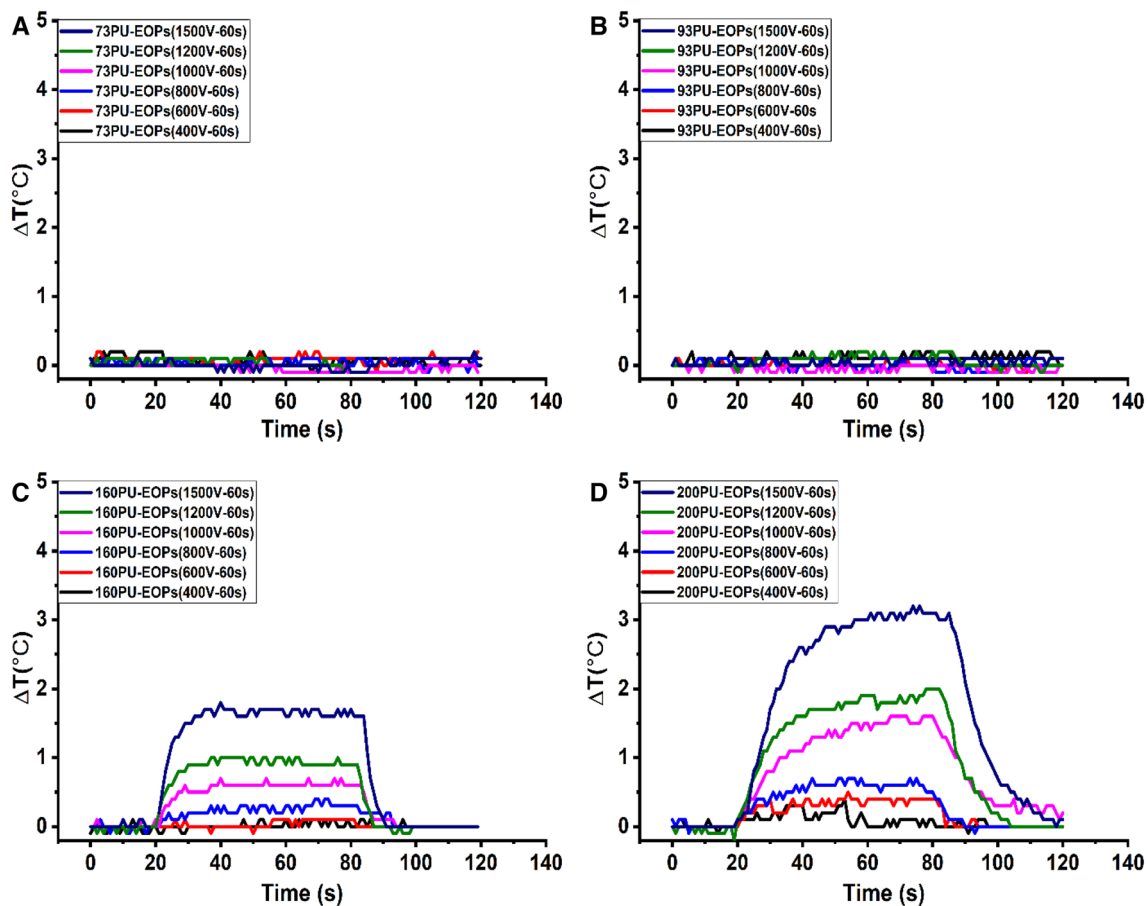


Fig. 7 The temperature difference of PU-EOPs with different diameters at different voltage (400–1000 V). **A** $73 \mu\text{m}$ -EOPs; **B** $93 \mu\text{m}$ -EOPs; **C** $160 \mu\text{m}$ -EOPs; **D** $200 \mu\text{m}$ -EOPs

heat generation. This also indicated that it could be advantageous to use small inner capillaries, when the temperature is the key factor that dramatically influences the performance of EOPs.

3.2.3 Flow rates of PU multi-capillary EOP

The flow rates of PU multi-capillary EOPs (based on fibres whose cross-sectional images are shown in Fig. 4) of 20 mm in length were investigated, Fig. 8. Here, the flow rates of the EOP experienced a significant increase with increasing voltage and demonstrated behaviour similar to the single capillary EOP configuration (Sect. 3.2.1). The maximum flow rate for EOP with an equivalent of 7* capillaries was 5.3 $\mu\text{L}/\text{min}$ at 1500 V, which was approximately double the rate of the 5-capillary EOP and nearly 7 times for 1-capillary EOP. The number of capillaries significantly affects the flow rates of EOP where the higher flow rates were achieved by the higher number of capillaries. The flow rates achieved here (5.3 $\mu\text{L}/\text{min}$ at 1500 V or $3.53 \times 10^{-3} \mu\text{L}/\text{min V}$) were greater than the reported Si-based microchannel devices with a flow rate of $6.00 \times 10^{-4} \mu\text{L}/\text{min V}$ (Heuck and Staufer 2011), similar to PDMS based microchannels with a flow rate of $2.84 \times 10^{-3} \mu\text{L}/\text{min V}$ (Ye et al. 2019), and lower than a reported PU microfluidic device with a 76.8 $\mu\text{L}/\text{min V}$ (Piccin et al. 2007) as shown in Table 1. It should be noted that the manufacturing techniques required to produce these Si-related, PDMS and PU devices were far more complex, compared to the simple fibre drawing approach adopted here.

From Eq. 5 (see ESI Sect. 1.1), the flow rate is related to the applied electric field (E), the cross-sectional dimensions (r), the working liquid, the surface charge density of the channel as well as the temperature. Increasing the number

of capillaries increases the cross-sectional area (dimensions), which increases the flow rate. Figure S4 shows the relationship between the flow velocity and the number of the capillaries (or the cross-sectional dimensions). For a given voltage, a working liquid and a well-distributed capillaries configuration, the flow velocity of PU multi-capillary EOP (m/min) was similar. As a result, increasing the number of capillaries did not boost the flow rate per capillary (area) but resulted in an increase in mass flow rates.

Additionally, the slight non-linear behaviour observed for the 7* capillary EOP was likely due to the non-uniform capillaries sizes and the difficulty in determining the actual flow contribution from the number of smaller capillaries. The cross-sectional area of each capillary shown in Fig. 4C was very different in this configuration, particularly where one capillary in the middle of the structure was calculated to have a cross-sectional area of $11 \times 10^3 \mu\text{m}^2$ which was three times the size of other capillaries in this layout. This non-uniformity likely resulted in the differing flow rates. Compounding this, Joule heating which arises from resistive heating of the multi-capillary with increasing capillary area also contributes to non-linear flow behaviour.

3.2.4 Further potential applications

In this study, simple, cost-effective, and scalable thermo-plastic PU capillary fibre-based electroosmotic pumps were successfully demonstrated to be feasible and reproducible. The results were very promising, however, at this proof-of-concept state, it leaves scope for optimisation, in particular, the potential applications.

One main application of using the PU capillaries to control fluid flow is for sample acquisition and analysis. Particularly, PU capillaries here can be an alternative to a reported polymethylmethacrylate (PMMA)-based microfluidic device with complex microchannels (Jubery et al. 2012) to process bio-separation and concentration tests based on isotachopheresis (ITP). Furthermore, the fabrication techniques required to produce PMMA channels were far more complex than the simple fibre drawing approach adopted here. Another aspect that PU capillaries and EOPs can be applied is to manipulate biological cells. *E. coli* and *S. cerevisiae* cells, for example, were used to study the electrokinetic transport in polymer-based microfluidic devices (Witek et al. 2004). Due to the fact that cells can be driven separately using electrophoretic/electroosmotic forces in a microchannel, PU capillary EOPs could be used as a microdevice for cells separation. In addition, due to the flexibility and stretchability of PU capillaries (microchannels) structures, PU capillary EOPs have great potential to be used into many areas including flexible microfluidic devices and flexible wearable electronics (Falahi et al. 2019).

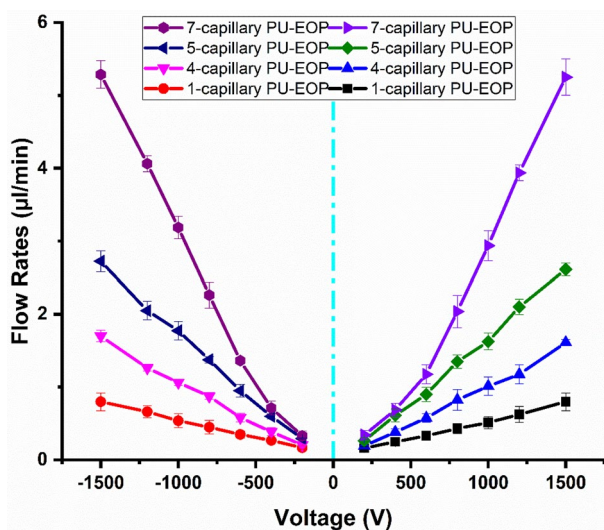


Fig. 8 The flow rates of multi-capillary PU-EOPs versus voltages

4 Conclusions

Simple, cost-effective and scalable capillary fibre-based electroosmotic pumps were successfully produced utilising a thermally drawn thermoplastic PU fibre drawing technique. Single capillary EOPs with internal diameters ranging from 73 to 200 μm were fabricated and were shown to be capable of actively transporting a buffer solution using a driving electric potential. Results show that a maximum flow rate of 0.8 $\mu\text{L}/\text{min}$ was achieved for a 73 μm diameter PU fibre at an applied potential of 750 V/cm. Furthermore, this flow rate was successfully increased up to 5.3 $\mu\text{L}/\text{min}$ by the drawing of a multi-capillary array consisting of up to 7* capillaries. Overall, the concept of creating PU capillary structures, using a simple and low-cost approach, for EOPs was shown to be feasible and reproducible, thereby opening up more opportunities in development of microfluidic devices.

Supplementary Information The online version contains supplementary material available at <https://doi.org/10.1007/s10404-022-02546-y>.

Acknowledgements The authors would like to acknowledge funding support from the Australian Research Council Centre of Excellence Scheme (CE 140100012) and the Australian Research Council Discovery Project DP170103537. The authors thank the Australian National Fabrication Facility (ANFF)—Materials Node and NSW Nodes for access to the facilities hosted at the University of Wollongong and the Research & Prototype Foundry Core Research Facility at the University of Sydney. The ANFF is funded through the National Collaborative Research Infrastructure Strategy (NCRIS) providing nano- and micro-fabrication facilities for Australia's researchers. We also gratefully acknowledge the technical assistance of Peter Henry and Justin Digweed.

Funding Open Access funding enabled and organized by CAUL and its Member Institutions.

Declarations

Conflict of interest The authors declare that they have no conflict of interest.

Open Access This article is licensed under a Creative Commons Attribution 4.0 International License, which permits use, sharing, adaptation, distribution and reproduction in any medium or format, as long as you give appropriate credit to the original author(s) and the source, provide a link to the Creative Commons licence, and indicate if changes were made. The images or other third party material in this article are included in the article's Creative Commons licence, unless indicated otherwise in a credit line to the material. If material is not included in the article's Creative Commons licence and your intended use is not permitted by statutory regulation or exceeds the permitted use, you will need to obtain permission directly from the copyright holder. To view a copy of this licence, visit <http://creativecommons.org/licenses/by/4.0/>.

References

- Aryasomayajula A, Bayat P, Rezai P, Selvaganapathy PR (2017) Microfluidic devices and their applications. In: Bhushan B (ed) Springer handbook of nanotechnology. Springer, Berlin, pp 487–536
- Atakaramians S, Argyros A, Fleming SC, Kuhlmeier BT (2012) Hollow-core waveguides with uniaxial metamaterial cladding: modal equations and guidance conditions. *J Opt Soc Am B* 29:2462–2477
- Chen L, Choo J, Yan B (2007) The microfabricated electrokinetic pump: a potential promising drug delivery technique. *Expert Opin Drug Deliv* 4:119–129
- Chen L, Ma J, Guan Y (2004) Study of an electroosmotic pump for liquid delivery and its application in capillary column liquid chromatography. *J Chromatogr A* 1028:219–226
- Cheng Y, Koh L-D, Li D, Ji B, Zhang Y, Yeo J, Guan G, Han M-Y, Zhang Y-W (2015) Peptide–graphene interactions enhance the mechanical properties of silk fibroin. *ACS Appl Mater Interfaces* 7:21787–21796
- Dasgupta PK, Liu S (1994) Electroosmosis: a reliable fluid propulsion system for flow injection analysis. *Anal Chem* 66:1792–1798
- Domansky K, Leslie DC, McKinney J, Fraser JP, Sliz JD, Hamkins-Indik T, Hamilton GA, Bahinski A, Ingber DE (2013) Clear castable polyurethane elastomer for fabrication of microfluidic devices. *Lab Chip* 13:3956–3964
- Eijkelenborg MAV, Large MCJ, Argyros A, Zagari J, Manos S, Issa NA, Bassett I, Fleming S, McPhedran RC, Sterke CMD, Nicorovic NAP (2001) Microstructured polymer optical fibre. *Opt Express* 9:319–327
- Eijkelenborg MAV, Argyros A, Bachmann A, Barton G, Large MCJ, Henry G, Issa NA, Klein KF, Poisel H, Pok W, Poladian L, Manos S, Zagari J (2004) Bandwidth and loss measurements of graded-index microstructured polymer optical fibre. In: *Electronics letters. Institution of Engineering and Technology*, pp 592–593
- Eng PF, Nithiarasu P, Guy OJ (2010) An experimental study on an electro-osmotic flow-based silicon heat spreader. *Microfluid Nanofluid* 9:787–795
- Fallahi H, Zhang J, Phan HP, Nguyen NT (2019) Flexible microfluidics: fundamentals, recent developments, and applications. *Micromachines (Basel)* 10(12):830–856. <https://doi.org/10.3390/mi10120830>
- Fan Y, Huang L, Cui R, Zhou X, Zhang Y (2020) Thermoplastic polyurethane-based flexible multilayer microfluidic devices. *J Micro/Nanolithogr MEMS MOEMS* 19:024501
- Farajikhah S, Runge AFJ, Boumelhem BB, Rukhlenko ID, Stefani A, Sayyar S, Innis PC, Fraser ST, Fleming S, Large MCJ (2021) Thermally drawn biodegradable fibers with tailored topography for biomedical applications. *J Biomed Mater Res B Appl Biomater* 109:733–743
- Farajikhah S, Rukhlenko I, Stefani A, Large M, Chrzanowski W, Fleming S (2019) Thermally drawn polycaprolactone fibres with customised cross sections, vol 11200, SPIE
- Fleming S, Stefani A, Tang X, Argyros A, Kemsley D, Cordi J, Lwin R (2017) Tunable metamaterials fabricated by fiber drawing. *J Opt Soc Am B* 34:D81–D85
- Gao M, Gui L (2014) A handy liquid metal based electroosmotic flow pump. *Lab Chip* 14:1866–1872
- Gao M, Gui L (2016) Development of a multi-stage electroosmotic flow pump using liquid metal electrodes. *Micromachines* 7:165
- Ghosal S (2004) Fluid mechanics of electroosmotic flow and its effect on band broadening in capillary electrophoresis. *Electrophoresis* 25:214–228
- Ghosal S (2006) Electrokinetic flow and dispersion in capillary electrophoresis. *Annu Rev Fluid Mech* 38:309–338

- Grushka E, McCormick RM, Kirkland JJ (1989) Effect of temperature gradients on the efficiency of capillary zone electrophoresis separations. *Anal Chem* 61:241–246
- Gunther A, Jensen KF (2006) Multiphase microfluidics: from flow characteristics to chemical and materials synthesis. *Lab Chip* 6:1487–1503
- Guo MT, Rotem A, Heyman JA, Weitz DA (2012) Droplet microfluidics for high-throughput biological assays. *Lab Chip* 12:2146–2155
- Hamblin JME, Fuentes MN, Peeni HV, Lee BA, Woolley ML, Hawkins AR (2007) Thin film electro-osmotic pumps for biomicrofluidic applications. *Biomicrofluidics* 1:014101
- Hayashi JG, Lwin R, Stefani A, Fleming S, Kuhlmeier BT, Argyros A (2019) Fabrication of soft-glass-based wire array metamaterial fibers for applications at infrared frequencies. *J Lightw Technol* 37:5001–5009
- Helmholtz H (1853) Ueber einige Gesetze der Vertheilung elektrischer Ströme in körperlichen Leitern mit Anwendung auf die thierisch-elektrischen Versuche. *Ann Phys* 165:211–233
- Henry AC, Waddell EA, Shreiner R, Locascio LE (2002) Control of electroosmotic flow in laser-ablated and chemically modified hot imprinted poly(ethylene terephthalate glycol) microchannels. *Electrophoresis* 23:791–798
- Heuck FCA, Staufer U (2011) Low voltage electroosmotic pump for high density integration into microfabricated fluidic systems. *Microfluid Nanofluid* 10:1317–1332
- Hosokawa K, Sato K, Ichikawa N, Maeda M (2004) Power-free poly(dimethylsiloxane) microfluidic devices for gold nanoparticle-based DNA analysis. *Lab Chip* 4:181–185
- Huang X, Gordon MJ, Zare RN (1988) Current-monitoring method for measuring the electroosmotic flow rate in capillary zone electrophoresis. *Anal Chem* 60:1837–1838
- Johnson TJ, Ross D, Locascio LE (2002) Rapid microfluidic mixing. *Anal Chem* 74:45–51
- Jubery TZ, Hossain MR, Bottenus DR, Ivory CF, Dong W, Dutta P (2012) A new fabrication technique to form complex polymethylmethacrylate microchannel for bioseparation. *Biomicrofluidics* 6:016503
- Kaysir MR, Stefani A, Lwin R, Fleming S (2017) Flexible optical fiber sensor based on polyurethane. In: 2017 conference on lasers and electro-optics Pacific rim. Optical Society of America, Singapore, p s1551
- Kirby BJ, Hasselbrink EF Jr (2004) Zeta potential of microfluidic substrates: 2. Data for polymers. *Electrophoresis* 25:203–213
- Kok WT (2000) Capillary electrophoresis: instrumentation and operation. *Chromatographia* 51:S1–S89
- Koster S, Angile FE, Duan H, Agresti JJ, Wintner A, Schmitz C, Rowat AC, Merten CA, Pisignano D, Griffiths AD, Weitz DA (2008) Drop-based microfluidic devices for encapsulation of single cells. *Lab Chip* 8:1110–1115
- Kudo H, Yonekawa T, Yoshimi S, Oguri Y, Tsukune A, Kim YS, Kitada H, Fjimoto K, Kinefuchi I, Matsumoto Y, Ohba T (2014) High-performance cooling system with multi-channel electroosmotic flow pumps for high-power 3D-ICs. In: 2014 international conference on electronics packaging, ICEP 2014, pp 480–483
- Lazar IM, Karger BL (2002) Multiple open-channel electroosmotic pumping system for microfluidic sample handling. *Anal Chem* 74:6259–6268
- Lim AE, Lim CY, Lam YC, Taboryski R (2018) Electroosmotic flow in microchannel with black silicon nanostructures. *Micromachines* 9:229
- Lion N, Rohner TC, Dayon L, Arnaud IL, Damoc E, Youhnovski N, Wu Z-Y, Roussel C, Jossierand J, Jensen H, Rossier JS, Przybylski M, Girault HH (2003) Microfluidic systems in proteomics. *Electrophoresis* 24:3533–3562
- Locascio LE, Perso CE, Lee CS (1999) Measurement of electroosmotic flow in plastic imprinted microfluid devices and the effect of protein adsorption on flow rate. *J Chromatogr A* 857:275–284
- Miller S, Weiss AA, Heineman WR, Banerjee RK (2019) Electroosmotic flow driven microfluidic device for bacteria isolation using magnetic microbeads. *Sci Rep* 9:14228
- Mohammadi M, Madadi H, Casals-Terré J (2015) Microfluidic point-of-care blood panel based on a novel technique: reversible electroosmotic flow. *Biomicrofluidics* 9:054106
- Nge PN, Rogers CI, Woolley AT (2013) Advances in microfluidic materials, functions, integration, and applications. *Chem Rev* 113:2550–2583
- Piccin E, Coltro WKT, Fracassi da Silva JA, Neto SC, Mazo LH, Carrilho E (2007) Polyurethane from biosource as a new material for fabrication of microfluidic devices by rapid prototyping. *J Chromatogr A* 1173:151–158
- Pittman JL, Henry CS, Gilman SD (2003) Experimental studies of electroosmotic flow dynamics in microfabricated devices during current monitoring experiments. *Anal Chem* 75:361–370
- Singh N, Tuniz A, Lwin R, Atakaramians S, Argyros A, Fleming SC, Kuhlmeier BT (2012) Fiber-drawn double split ring resonators in the terahertz range. *Opt Mater Express* 2:1254–1259
- Sun Y, Lim CS, Liu AQ, Ayi TC, Yap PH (2007) Design, simulation and experiment of electroosmotic microfluidic chip for cell sorting. *Sens Actuators A* 133:340–348
- Tuniz A, Kaltenecker KJ, Fischer BM, Walther M, Fleming SC, Argyros A, Kuhlmeier BT (2013) Metamaterial fibres for subdiffraction imaging and focusing at terahertz frequencies over optically long distances. *Nat Commun* 4:2706
- Wainright A, Nguyen UT, Bjornson T, Boone TD (2003) Preconcentration and separation of double-stranded DNA fragments by electrophoresis in plastic microfluidic devices. *Electrophoresis* 24:3784–3792
- Wang X, Cheng C, Wang S, Liu S (2009a) Electroosmotic pumps and their applications in microfluidic systems. *Microfluid Nanofluid* 6:145
- Wang X, Wang S, Gendhar B, Cheng C, Byun CK, Li G, Zhao M, Liu S (2009b) Electroosmotic pumps for microflow analysis. *Trends Anal Chem* 28:64–74
- Whitesides GM (2006) The origins and the future of microfluidics. *Nature* 442:368–373
- Witek MA, Wei S, Vaidya B, Adams AA, Zhu L, Strykowski W, McCauley RL, Soper SA (2004) Cell transport via electromigration in polymer-based microfluidic devices. *Lab Chip* 4:464–472
- Wu L, Beirne S, Cabot JM, Paull B, Wallace GG, Innis PC (2021) Fused filament fabrication 3D printed polylactic acid electroosmotic pumps. *Lab Chip* 21:3338–3351
- Wu W-I, Sask KN, Brash JL, Selvaganapathy PR (2012) Polyurethane-based microfluidic devices for blood contacting applications. *Lab Chip* 12:960–970
- Xuan X (2008) Joule heating in electrokinetic flow. *Electrophoresis* 29:33–43
- Yager P, Edwards T, Fu E, Helton K, Nelson K, Tam MR, Weigl BH (2006) Microfluidic diagnostic technologies for global public health. *Nature* 442:412–418
- Ye Z, Zhang R, Gao M, Deng Z, Gui L (2019) Development of a high flow rate 3-D electroosmotic flow pump. *Micromachines (basel)* 10:112